



Use of ENVISAT/ASAR wide-swath data for timely rice fields mapping in the Mekong River Delta

Alexandre Bouvet, Thuy Le Toan

► To cite this version:

Alexandre Bouvet, Thuy Le Toan. Use of ENVISAT/ASAR wide-swath data for timely rice fields mapping in the Mekong River Delta. Remote Sensing of Environment, 2011, 115 (4), pp.1090-1101. <10.1016/j.rse.2010.12.014>. <hal-00563142>

HAL Id: hal-00563142

<https://hal.science/hal-00563142v1>

Submitted on 4 Feb 2011

HAL is a multi-disciplinary open access archive for the deposit and dissemination of scientific research documents, whether they are published or not. The documents may come from teaching and research institutions in France or abroad, or from public or private research centers.

L'archive ouverte pluridisciplinaire **HAL**, est destinée au dépôt et à la diffusion de documents scientifiques de niveau recherche, publiés ou non, émanant des établissements d'enseignement et de recherche français ou étrangers, des laboratoires publics ou privés.



HAL Authorization

1 **USE OF ENVISAT/ASAR WIDE-SWATH DATA**
2 **FOR TIMELY RICE FIELDS MAPPING IN THE MEKONG RIVER DELTA**

3
4 **Alexandre Bouvet⁽¹⁾, Thuy Le Toan⁽¹⁾**

5
6 ***(1) Centre d'Etudes Spatiales de la Biosphère (CESBIO)***

7 ***18 Avenue Edouard Belin, 31401 Toulouse Cedex 9, France***

8 ***Email: Alexandre.Bouvet@gmail.com***

9
10 **Abstract:**

11 Because of the importance of rice for the global food security and because of the role of
12 inundated paddy fields in greenhouse gases emissions, monitoring the rice production world-
13 wide has become a challenging issue for the coming years. Local rice mapping methods have
14 been developed previously in many studies by using the temporal change of the backscatter from
15 C-band synthetic aperture radar (SAR) co-polarized data. The studies indicated in particular the
16 need of a high observation frequency. In the past, the operational use of these methods has been
17 limited by the small coverage and the poor acquisition frequency of the available data (ERS-1/2,
18 Radarsat-1). In this paper, the method is adapted for the first time to map rice at large scale, by
19 using wide-swath images of the Advanced SAR (ASAR) instrument onboard ENVISAT. To
20 increase the observation frequency, data from different satellite tracks are combined. The
21 detection of rice fields is achieved by exploiting the high backscatter increase at the beginning of
22 the growing cycle, which allows the production of rice maps early in the season (in the first 50
23 days). The method is tested in the Mekong delta in Vietnam. The mapping results are compared

to existing rice maps in the An Giang province, with a good agreement (higher than 81%). The rice planted areas are retrieved from the maps and successfully validated with the official statistics available at each province ($R^2=0.92$). These results show that the method is useful for large scale early mapping of rice areas, using current and future C band wide-swath SAR data.

I. INTRODUCTION

Rice is the staple food for more than half of humanity. Global rice production has increased continuously in the last half-century, since the Green Revolution. In the same period, the use of chemical inputs, the introduction of modern high-yielding varieties with short growing cycles, and the increased access to machinery and irrigation systems have led to a linear growth of the crop yields (+0.05ton/ha/year) according to the FAO (Food and Agriculture Organization of the United Nations 2009) as well as to an increase of the number of crops per year. This higher cropping intensity (from single to double or triple crop) together with the conversion of non-arable land to arable land have resulted in a drastic increase of rice harvested areas in the 60s and 70s (+1.4Mha/year) which slowed down in the 80s and 90s (+0.46Mha/year) and has tended to stabilize over the last ten years as a result of approaching the limits of land use and of cropping intensity, however with a large inter-annual variability due to climatic conditions and socio-economic factors. As both the increase in yield and in planted areas will be facing limitations in the next decades, it is unlikely that rice production can keep increasing at the same rate. Meanwhile, world population, and therefore demand for food, has increased linearly over the last fifty years (+80M/year), and is projected to keep growing until around 2050 up to 9 billion inhabitants (United Nations Department of Economic and Social Affairs, Population

Division 2004). This conjuncture is prone to create tensions in food markets that could lead to world food price crises - as in April 2008 when the price of rice has more than doubled in only seven months - and eventually to famines. In this context of price instability and threatened food security, tools to monitor rice production in real-time are highly needed by governments, traders and decision makers.

Moreover, rice agriculture is strongly involved in various environmental aspects, from water management to climate change due to the high emissions of methane. For this reason, a longer-term inter-annual monitoring is also required in order to study the impact of the changes in rice areas and in cultural practices that are likely to occur in the next years to face the economic and environmental context.

Satellite remote sensing data offer a unique possibility to provide frequent and regional to global-scale observations of the Earth over a long period (the lifespan of a satellite is around 10 years, and satellites are launched regularly to provide continuity in the data).

Optical sensors are seriously limited by frequent cloud cover in tropical and sub-tropical areas where rice is grown in majority. A study combining agricultural census data and a large dataset of Landsat TM imagery allowed producing maps of the distribution of rice agriculture in China at a 0.5° spatial resolution (Frolking et al. 2002). However, to achieve the coverage of such a large area with high-resolution (30m) optical images, a consequent amount of data (520 scenes) had to be collected over a period of two years, which makes the method unsuitable for the production of timely statistics or yearly results. Because of the need of a high temporal observation frequency to get enough cloud-free images, a frequent global coverage can be ensured only through the use of medium resolution (around 250m-1km) sensors, such as the

MODerate resolution Imaging Spectrometer (MODIS), VEGETATION, or the MEdium Resolution Imaging Spectroradiometer (MERIS). The joint analysis of time-series of vegetation and water indices derived from these sensors, such as the Normalized Difference Vegetation Index (NDVI), the Enhanced Vegetation Index (EVI), or the Normalized Difference Water Index (NDWI), also known as the Land Surface Water Index (LSWI), exhibits a specific temporal behaviour during flooding of rice paddies and transplanting of rice plants. This feature has been exploited to map the spatial distribution of rice agriculture at large scales in China using VEGETATION (Xiao et al. 2002a; Xiao et al. 2002b) and MODIS (Xiao et al. 2005), and in South and South-East Asia using MODIS (Xiao et al. 2006). Although these methods have produced very valuable outputs, none of them allows the retrieval of planted areas without the use of ancillary data. Indeed, because of the large number of mixed pixels at such spatial resolutions, the fractional cover of rice in each pixel classified as rice had to be estimated through the use of high-resolution Landsat TM imagery (Xiao et al. 2002b; Xiao et al. 2005). Also, in (Xiao et al. 2006), the cropping intensity had to be derived from national agricultural statistics datasets, and the rice distribution in the Mekong River Delta was not properly reported according to the authors, probably because the flood pattern misleads the rice detection algorithm. The spatio-temporal distribution of rice phenology in the Mekong River Delta has been accurately estimated by an harmonic analysis of EVI time profiles from MODIS (Sakamoto et al. 2006). However, this method is not able to discriminate rice from other crops or vegetation types, and a prior identification of rice fields - e.g. by existing databases - is therefore needed.

Radar imaging systems, contrarily to optical sensors, have an all-weather capacity. The radar data are also well adapted to distinguish rice from other land cover types because of the specific

93 response of the radar backscattering of inundated vegetation. The interaction between a radar
94 electromagnetic wave and vegetation involves mainly three mechanisms: the volume scattering,
95 the scattering from the ground attenuated by the vegetation canopy, and the multiple scattering
96 between the volume and the ground. The last term brings a negligible contribution compared to
97 the two others in the usual case of vegetation growing over non-flooded soils. However, in the
98 case of flooded fields such as rice paddies, this term becomes dominant when the plants develop
99 because of the double-bounce between the plant stems (which are the dominant scatterers in the
100 volume) and the water surface. This has been demonstrated by theoretical models for the case of
101 C-band co-polarized (HH or VV) backscatter at 23° incidence angle (Le Toan et al. 1997; Wang
102 et al. 2005). This volume-ground interaction (double-bounce) is responsible for the first of the
103 two main properties of the rice backscatter: the backscattering intensity at polarizations HH and
104 VV show a significant increase during the vegetative phase, right after the low values of the
105 flooding stage, and then decrease slightly during the reproductive phase until harvest. This
106 backscatter increase in rice fields was generally observed from ERS, RADARSAT-1 or ASAR
107 to be superior to 8 dB, and sometimes much more (Chakraborty et al. 2005; Chen et al. 2007;
108 Kurosu et al. 1995; Shao et al. 2001). Scatterometer measurements on an experimental paddy
109 field in Japan have shown that this high backscatter increase is observed not only at C-band but
110 also at X-band and L-band (Inoue et al. 2002). For L-band however, other studies demonstrated
111 that in the case of mechanically planted fields, this increase is smaller (3-4 dB) except in specific
112 configurations of the plant rows (orientation and spacing) where resonant scattering leads to
113 extreme backscatter increases of more than 20 dB (Rosenqvist 1999). This dependence on the
114 plant row configuration limits the usefulness of L-band data for operational applications at wide-
115 scale.

The vertical structure of the rice plants is responsible for the second property of the rice backscatter: the vertically polarized wave is more attenuated than the horizontally polarized wave, and for that reason the ratio of the HH and VV backscatter intensities is higher than that of most other land cover classes, reaching values around 6-7dB according to a joint analysis of ERS and RADARSAT-1 data (Le Toan et al. 1997; Ribbes and Le Toan 1999) and to the modelling of C-band HH and VV (Le Toan et al. 1997; Wang et al. 2005). The same is observed at X-band (Le Toan et al. 1989).

The rice fields mapping methods based on SAR data that have been developed so far mainly rely on these two properties of rice fields. The first property (high backscatter increase during rice growing season) has been exploited in classification algorithms using the temporal change of co-polarized backscatter as a classification feature, mostly at C-band, in various Asian countries (Chen and McNairn 2006; Le Toan et al. 1997; Liew et al. 1998; Ribbes and Le Toan 1999). The second property (high HH/VV polarization ratio) has led to the development of methods using this polarization ratio as a classification feature, at C-band in Vietnam (Bouvet et al. 2009) and at X-band in Spain (Lopez-Sanchez et al. 2010). All these rice mapping schemes have proven effective but have been applied only at local scales, with high resolution (less than 50 m) data. The use of these methods and data to map rice on larger areas (regional to continental scales) would require the acquisition and processing of a dissuasive amount of high resolution data. The existence of wide-swath sensors in current (ASAR, RADARSAT-2, PALSAR) or future (Sentinel-1, RISAT-1) systems opens the way to the adaptation of these methods to medium-resolution (50-100m) data for the mapping of rice areas at large scale. However, no satellite wide-swath data with dual-polarization HH and VV capability is available so far, so only the methods based on backscatter temporal change can be considered.

The present study aims at developing an operational method for the early assessment of rice planted areas using medium-resolution wide-swath single-polarization SAR imagery, by exploiting the outstanding temporal behaviour of rice backscattering. Because of the limitations of L-band in mechanically planted fields and because of the absence of wide-swath sensors operating at X-band, we choose to use C-band data. Section II describes the test site and the data used in the study. The mapping method is developed in Section III. Section IV presents the mapping results and their validation.

II. SITE AND DATA

A. Site description

The study site is the Mekong Delta, the major rice-producing area in Vietnam. It produces more than half of the rice in Vietnam, thus accounting for around 3% of the world production.

The Mekong Delta is a region constituted by 13 provinces in the southern tip of the country, covering around 40000 km² (275km from North to South, 260km from West to East), where the Mekong River approaches and empties into the South China sea through a network of nine main distributaries. The topography is very flat, with most of the land below 5m. Figure 1 presents the locations and names of the 13 provinces and the topography of the area from the Shuttle Radar Topography Mission (SRTM) Digital Elevation Model (DEM). The climate is tropical (8.5°N-11°N in latitude), with the wet season starting in May and lasting until October-November, and the dry season from December to April. Seasonal floods occur in a large part of the area, starting in August in the upper Delta, then spreading to the lower Delta, peaking in September-October and lasting until the beginning of December. The floods bring large amounts of silt that

contribute to the fertilization of the soil. The land is dedicated mostly to agriculture (63%), aquaculture (17.7%) and forestry (8.9%) (General Statistics Office of Vietnam 2006), with the agricultural land comprising predominantly rice paddies (76%), as well as orchards, sugarcane and annual crops (General Statistics Office of Vietnam 2009). The delta is therefore a rural, but very densely populated area, with 17.7 million inhabitants.

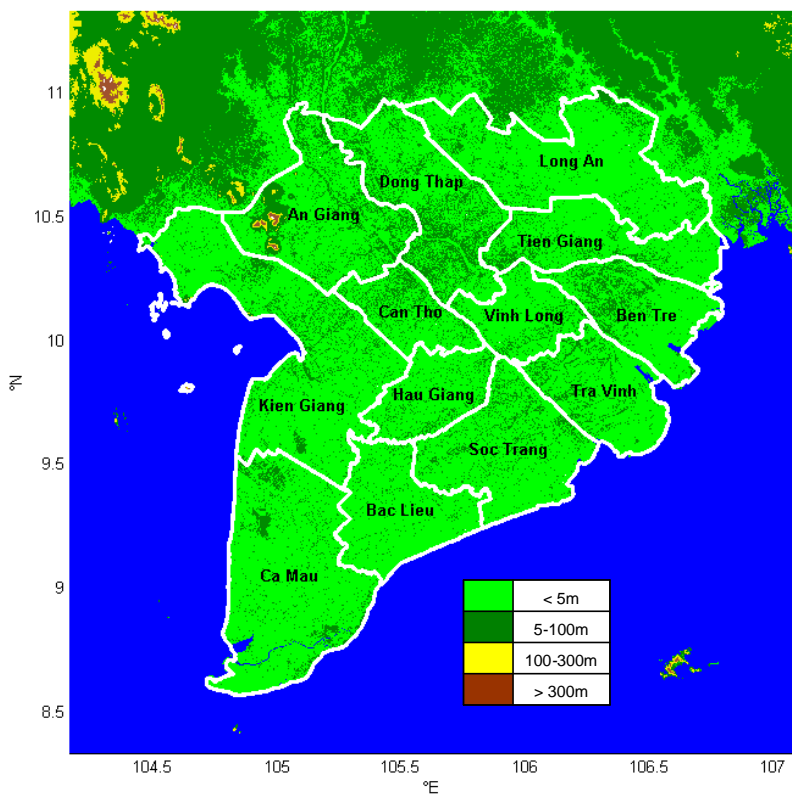


Figure 1. Map of the 13 provinces in the Mekong River Delta and topography from SRTM.

The rice cultivation pattern is quite complex. Originally, floating rice paddies were cultivated and, being dependent on rainfall and seasonal floods, only one crop of rice was harvested every year, during the wet season. However, in the last decades, the introduction of modern varieties, with higher yields and a shorter growth cycle, and technical components such as chemical

175 fertilizers, pesticides, machinery and low-lift pumps together with the development of canal
176 networks have led to the intensification of paddy agriculture, allowing to grow two or sometimes
177 three crops of rice per year (Tanaka 1995).

178 The land can be divided roughly into two ecological types: inland areas and coastal areas. Inland
179 areas are covered with a dense irrigation network and benefit from a fertile soil thanks to the
180 sediments brought by the floods, which allow double or triple-cropping of rice. They are formed
181 by inland provinces: An Giang, Đồng Tháp, Cần Thơ, Hậu Giang, Vĩnh Long, the western part
182 of Tiền Giang, and Long An. Coastal areas are prone to salt intrusion in the dry season which
183 limits the soil fertility. The major cropping patterns are therefore single rice with shrimp farming
184 or double rice. This concerns part or all of the coastal provinces: Kiên Giang, Cà Mau, Bạc Liêu,
185 Sóc Trăng, Trà Vinh and Bến Tre.

186

187 In inland areas, one crop of rice is grown during the dry season. This “Winter-Spring” rice
188 (locally called “Đông Xuân”) is planted in November-December and harvested between
189 February and April. In the wet season, farmers grow one or two crops of rice. The “Summer-
190 Autumn” crop (locally named “Hè Thu”) is planted in April-early June and harvested in July-
191 early August. When the fields are protected from seasonal floods (dykes have been built after the
192 2000 record floods), a second wet-season crop is grown. This “Autumn-Winter” rice (locally
193 named “Thu Đông”) is transplanted in August and harvested in November-December.

194 In coastal areas where saline intrusion limit the number of rice crops per year, one Summer-
195 Autumn rice is grown and a second crop in the “Main wet season” (locally called “Mùa”), which
196 is planted from July to August and harvested from November to February, i.e. with a variable
197 calendar between early, medium and late fields.

Table 1 sums up the information related to these seasons. Rice seasons are numbered according to their order of occurrence in the civil year.

Table 1. Rice agricultural seasons in the Mekong Delta River

| Season number | English name | Vietnamese name | Planting date | Harvest date | Distribution |
|---------------|-----------------|-----------------|---------------|--------------|--------------------|
| 1 | Winter-Spring | Đông Xuân | Nov-Dec | Feb-Apr | inland |
| 2 | Summer-Autumn | Hè Thu | Apr-Jun | Jul-Aug | inland and coastal |
| 3a | Autumn-Winter | Thu Đông | Aug | Nov-Dec | inland |
| 3b | Main wet season | Mùa | Jul-Aug | Nov-Feb | coastal |

B. Statistical data

The mapping methods developed in this paper will be validated through the comparison of the planted areas retrieved from the remote sensing methods to the planted areas reported in the official national statistical data.

The statistical system in Vietnam is centralized. Statistical data are collected first at the commune level, and then aggregated at the district, province and finally country level by the corresponding statistics offices. For obvious practical reasons, most of the agricultural statistics are based on sampling at the district level, rather than on an exhaustive census. For the specific case of rice planted areas, a three-stage sampling is applied in each district, at the commune, village, and farming household levels. For the retained communes, enumerators report to the District Statistics Offices the rice planted areas in the fields owned by the selected farming

households in the selected villages. The collected data are then forwarded to the Province Statistics Offices, and finally the General Statistics Office (GSO) (Food and Agriculture Organization of the United Nations 2002). Around 100000 farming households in the whole country are involved in the rice area sampling, out of a total of more than 9 million households that grow paddy (Food and Agriculture Organization of the United Nations 2002). This hierarchical acquisition scheme is very time- and resource-consuming. Moreover, its accuracy is intrinsically limited by the errors consecutive to the sampling.

The General Statistics Office publishes annual agricultural statistics for each of the 58 provinces and 5 centrally-controlled municipalities in Vietnam. For paddy rice agriculture, these statistics comprise planted area, production and yield. The different crops of rice are gathered into three categories: Spring (labelled as “Đông Xuân” in the Vietnamese database), Autumn (“Hè Thu”) and Winter (“Mùa”) seasons. The figures for each of these three seasons in 2007 for every province of the Mekong River Delta are presented in Table 2.

Table 2. Planted area of rice by province for the three rice seasons in 2007 from national statistics

| | Planted area in 2007 (ha) | | |
|-------------------|---------------------------|--------|--------|
| | Spring | Autumn | Winter |
| Long An | 234300 | 178800 | 15400 |
| Tiền Giang | 83400 | 163400 | 0 |
| Bến Tre | 20700 | 24200 | 34800 |
| Trà Vinh | 49700 | 81100 | 93200 |
| Vĩnh Long | 68500 | 89800 | 0 |

| | | | |
|-------------------|---------|---------|--------|
| Đồng Tháp | 208400 | 238700 | 0 |
| An Giang | 230600 | 282700 | 7300 |
| Kiên Giang | 265300 | 266500 | 51200 |
| Cần Thơ | 92100 | 115800 | 0 |
| Hậu Giang | 79000 | 110300 | 0 |
| Sóc Trăng | 140700 | 158900 | 25900 |
| Bạc Liêu | 33900 | 53300 | 62600 |
| Cà Mau | 0 | 36000 | 87100 |
| Total | 1506600 | 1799500 | 377500 |

The correspondence between these three categories (Spring, Autumn, and Winter) and the agricultural seasons presented in the previous sub-section (Winter-Spring, Summer-Autumn, Autumn-Winter, and Main wet season) is not straightforward, and has to be discussed. The diversity of harvesting time and the differences in rice cropping patterns from the North to the South of Vietnam tend to make such a countrywide categorization irrelevant.

Figure 2 shows the proportion of each of the Spring, Autumn and Winter crops that are planted in each province in 2007 according to the statistics. The inland provinces grow mostly Spring and Autumn crops, with no or very few Winter crop, which seems paradoxical at first sight as triple-cropping is practised in these regions. The planted area for Autumn rice is higher than for Spring rice in the statistics, while in reality, the Winter-Spring and Summer-Autumn planted areas are similar, with the Autumn-Winter coming as an optional third crop in a small number of fields. Therefore, it can be assumed that in the inland provinces, the Spring statistical category accounts for the Winter-Spring crop, and the Autumn category for the sum of the Summer-

Autumn and Autumn-Winter crops. Reversely, the coastal provinces grow the three kinds of rice (except Cà Mau with no Spring rice), while the dominant patterns are single and double-cropping, with marginal areas growing irrigated triple-rice, especially in Soc Trang. It can then be inferred that, in the coastal provinces, the Spring category represents the Winter-Spring rice, the Autumn category corresponds to the Summer-Autumn rice and the Winter category gathers the main wet season (Mua) from the double-rice pattern and the Autumn-Winter season from the triple-rice pattern. Therefore, it seems that the three rice seasons described in the statistics do not cover the same categories in the coastal provinces and in the inland provinces. Table 3 gives a synthetic view of the supposed correspondence between these seasons from the statistical database and the agricultural seasons from Table 1.

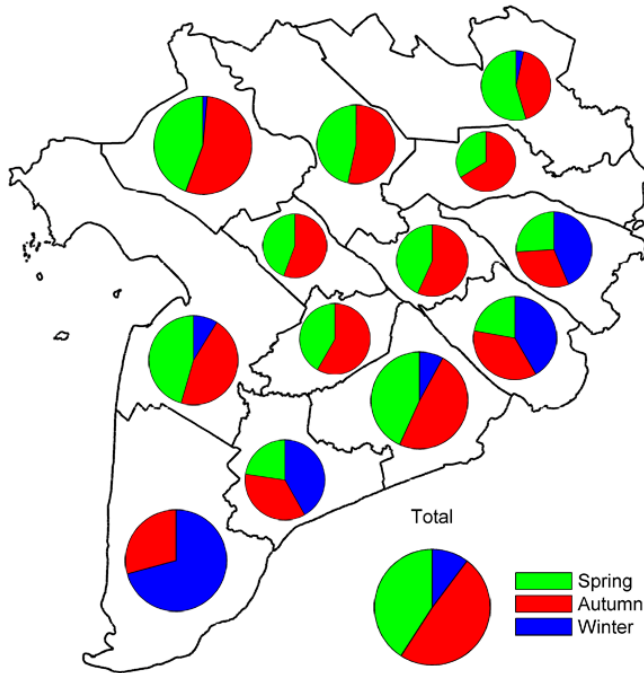


Figure 2. Proportion of Spring, Autumn and Winter rice planted in each province in 2007.

Table 3. Correspondence between seasons from the statistical database and agricultural seasons.

| English name | Vietnamese name | Correspondence with agricultural seasons | |
|-----------------|--------------------|--|-------------------|
| | | Inland provinces | Coastal provinces |
| Spring | Đông Xuân | 1 | (1) |
| Autumn | Hè Thu | 2 + 3a | 2 |
| Winter | Mùa | (3b) | (3a) + 3b |

C. ASAR APP rice seasons map for An Giang province data

In a previous work (Bouvet et al. 2009), maps of the rice planted areas have been produced at a spatial resolution of 30m for the three rice seasons in 2007 in the province of An Giang. These maps have been obtained by applying a 3dB threshold on the polarization ratio HH/VV on a time-series of ASAR Alternating Polarization Precision image (APP) data at incidence IS2 (19.2°-26.7°). The results have been validated using a land-use Geographic Information System (GIS) database covering one district, leading to a pixel-based accuracy of 89.9%. Moreover the estimated rice area in the Winter-Spring season for the whole province (229694 ha) has been compared to the preliminary statistics from the GSO (224273 ha), with a 2.4% difference between the two figures.

These maps will be used complementarily to the statistical data for further validation of the new methods presented in this paper.

D. ASAR WSM data

The ASAR instrument is a C-band SAR instrument (5.6cm wavelength) onboard the European satellite ENVISAT, which was launched in 2002, with multiple resolution, incidence, and polarization ability. Among the five operating modes of ASAR (Image Mode, Alternating Polarization, Wide Swath Mode, Wave Mode and Global Monitoring), only the Wide Swath Mode, using the ScanSAR technique, offers a wide enough swath (around 400km) with a spatial resolution adapted to accurate regional monitoring (around 150m, with a pixel spacing of 75m). The incidence angle in each image ranges from 17° to 42°.

Extensive time-series of Wide Swath mode Medium resolution (WSM) data have been acquired during the year 2007 over the Mekong Delta, with polarization HH, in order to monitor rice agriculture by means of methods based on the backscatter temporal change.

Studies on the assessment of classification methods based on temporal change (Bouvet et al. 2010) and previous studies using RADARSAT (Ribbes and Le Toan 1999) have emphasized the necessity of a high temporal observation frequency (e.g. around every ten days) to achieve acceptable classification accuracy. The time lapse between repeat-pass orbits of ENVISAT is 35 days. In order to increase the observation frequency, data from three different satellite tracks have been ordered: tracks 32 and 304 in descending pass and track 412 in ascending pass. Each of the three tracks covers the delta entirely, as can be seen in Fig. 3. The other tracks that would have covered the whole area have been left for the acquisition of Alternating Polarization data.

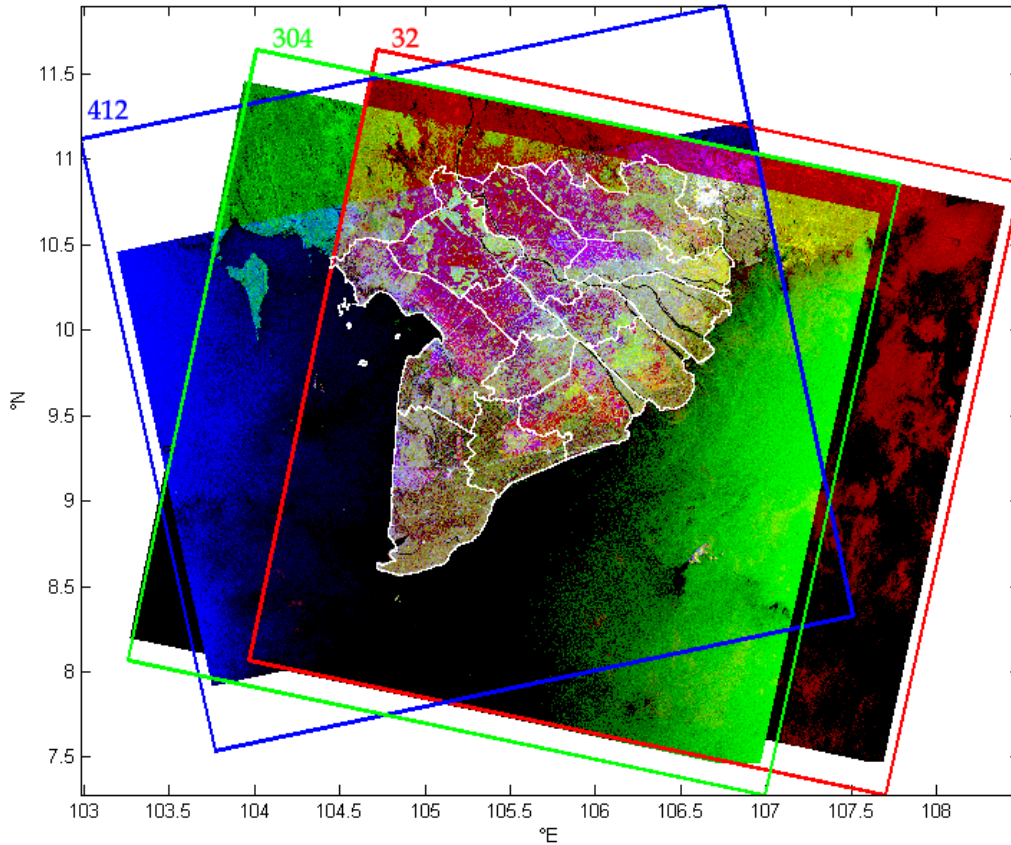


Figure 3. Colour-composite image of three WSM data from the three acquired tracks, with ascending tracks 32 and 304 in red and green respectively, and descending track 412 in blue.

The frames of the three tracks are presented in the corresponding colours.

The data acquisition sequence is the following: track 304, track 412, track 32 in intervals of respectively 7 and 9 days, followed by the next sequence 19 days later. Therefore, in this three-track configuration, the biggest time-lapse between two consecutive observations is 19 days, with a mean acquisition interval of 11.7 days. The improvement is thus significant compared to the single track acquisition frequency of one image every 35 days.

Table 4 lists the available dates for the three tracks. Track 412 is the most complete, with all the 2007 satellite passes successfully acquired. The last acquisition for track 304 is missing, and the dataset for track 32 is incomplete, with only 6 acquisitions.

Table 4. List of available dates in each track. Hyphens (-) indicate missing acquisitions.

| 304 | 412 | 32 |
|--------------|--------------|------------|
| 9 January | 16 January | - |
| 13 February | 20 February | 1 March |
| 20 March | 27 March | 5 April |
| 24 April | 1 May | 10 May |
| 29 May | 5 June | 14 June |
| 3 July | 10 July | 19 July |
| 7 August | 14 August | - |
| 11 September | 18 September | - |
| 16 October | 23 October | 1 November |
| - | 27 November | - |

The acquisition dates of the three tracks are plotted in Fig. 4 together with the agricultural seasons of the rice calendar described in II.A

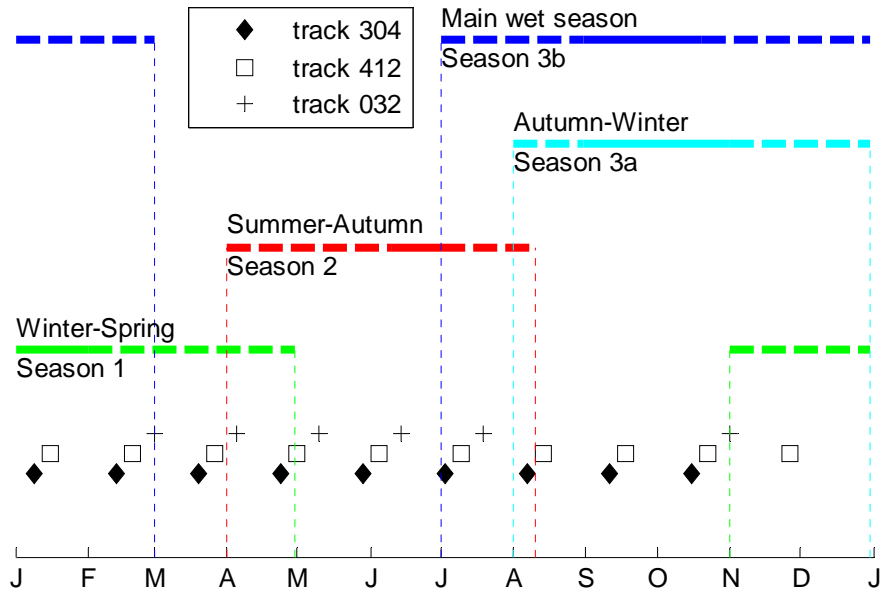


Figure 4. Rice calendar in the Mekong delta and dates of the available ASAR WSM data. For each rice crop, dashed lines represent the periods during which the beginning and the end of the crop can take place (spatial and interannual variability).

The conditions under which observations from different looking angles can be used together are discussed in the next section.

The pre-processing of the WSM data is done with the Gamma GEO software (Gamma Remote Sensing, Switzerland) and consists in the calibration of the SAR data and its geocoding with the elevation data from the DEM of SRTM at 3 arcseconds, and projected to lat/lon coordinates at the resolution of SRTM, corresponding to around 92m per pixel in latitude and longitude.

III. MAPPING METHOD

A. Rationale

The principle of this rice mapping method is to detect rice areas through the increase of their co-polarized backscatter intensity between two repeat-pass acquisitions when the first acquisition occurs at the flooding stage, i.e. when the backscatter is low because of the specular reflection over water, and the second acquisition occurs when the rice plants have started to grow, i.e. when the double-bounce provides high backscatter. Other classes are expected to remain relatively stable in comparison. The method has already proven effective at 23° incidence and HH or VV polarizations in past studies. The innovative aspect relies here in the use of multi-track acquisitions to increase the observation frequency and in the use of wide-swath data to ensure a regional coverage. For each pixel, the local incidence angle is different for the three tracks, and within one image, the incidence angles varies from 17° in the near range to 42° in the far range. The conditions under which such heterogeneous data can be used together have to be examined so as to develop a classification method that is invariant to the temporal and spatial variation in the incidence angle. The scatterometer measurements presented in (Inoue et al. 2002) and already mentioned in the introduction have been conducted at 25°, 35°, 45° and 55° incidence. This study has shown that the value of C-band HH backscatter changes with the incidence for a given phenological stage. A classification feature based on the value of the backscattering intensity is thus unsuitable for the case of wide-swath data from different tracks. For example, the detection of flooded fields by applying a threshold on the HH images to identify the low backscatter areas would not be relevant because the threshold would have to change with the local incidence angle within an image and between tracks. However, the

backscatter increase from flooding and transplanting to heading exceeds 9dB under any incidence angle. A classification feature based on a measurement of the temporal increase of backscatter between two consecutive acquisitions within a single track would therefore be efficient to map rice regardless of the track and regardless of the location of the pixel in the image. The temporal change is preferably measured by the ratio of intensities between two dates (i.e. the difference in dB) rather than by the difference of intensities, the latter producing larger classification errors in regions with a high backscatter than in regions with a low backscatter, contrarily to the former for which the classification error is independent on the backscatter intensity (Rignot and van Zyl 1993). Multi-track and multi-temporal classification features based on the combination of temporal intensity ratios will therefore be developed in this paper for the detection of rice fields.

B. Algorithm description

Computing the ratio of two SAR intensity images enhances the incertitude due to speckle. It is therefore necessary to reduce the speckle noise before producing ratio images. In this study, the backscatter images have been spatially filtered using an enhanced Lee filter (Lopes et al. 1990) implemented in the ENVI software (ITT Visual Information Solutions), with a 5×5 window size. The initial number of looks of the data is 3 in azimuth and 7 in range. The equivalent number of looks, defined as $\text{mean}^2/\text{variance}$, is calculated to be around 12 in the geocoded WSM images, and around 150 in the filtered images.

Figure 5 is a synoptic view of the different steps involved in the mapping algorithm, which will be described in the following sub-sections.

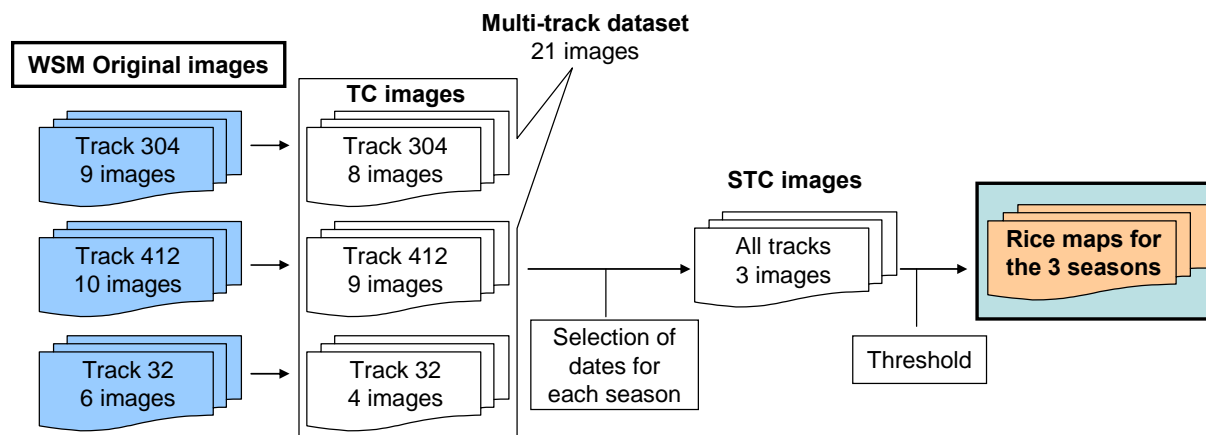


Figure 5. Synoptic view of the mapping algorithm.

Out of the twenty-five WSM images available in 2007, temporal change (TC) images are created by computing the ratio between two spatially filtered backscatter intensity images acquired within a track and separated by one satellite repeat pass (35 days): $TC = HH_{d+35} / HH_d$. These TC images compose a multi-track dataset of twenty-one images: eight from track 304, nine from track 412, and four from track 32.

The mapping algorithm consists in applying a threshold on these TC images in order to detect the rice fields that are flooded at the corresponding dates, characterized by their post-flooding backscatter increase. To detect all the rice areas planted during one season, one single TC image may however not be enough, because of shifts in the planting calendar, even within a province. The rice maps retrieved from the TC images must therefore be aggregated to produce seasonal maps. This is equivalent to applying the threshold directly on a seasonal temporal change (STC) classification feature, made up by taking the maximum value of the TC images among the dates corresponding to each season. The next sub-sections discuss how the threshold should be chosen, and how the dates corresponding to each season and each province can be selected. The

study will be conducted for Season 2 and Season 3 only, as the complete mapping of Season 1 (Winter-Spring) would require data from the end of 2006.

C. Defining the value of the classification threshold

Under the assumption of gamma distributed SAR intensities and uncorrelated images, a theoretical expression of the optimal classification threshold t_{opt} can be found for the two-class problem - a rice class and a non-rice class - when the classification feature is a single TC image (Bouvet et al. 2010):

$$t_{opt} = \sqrt{TC_{nr} TC_r} \cdot \frac{\sqrt{\frac{TC_r}{TC_{nr}}} \left(\frac{p(nr)}{p(r)} \right)^{\frac{1}{2L}} - 1}{\sqrt{\frac{TC_r}{TC_{nr}}} - \left(\frac{p(nr)}{p(r)} \right)^{\frac{1}{2L}}} \quad (1)$$

where nr and r denote respectively the non-rice and the rice classes, and $p(nr)$ and $p(r)$ denote the *a priori* probabilities of the non-rice class and of the rice class, i.e. the percentage cover of non-rice and rice in the landscape. TC_{nr} and TC_r represent the mean temporal change $\langle HH_{d+35} \rangle / \langle HH_d \rangle$ of the non-rice and the rice classes ($TC_r > TC_{nr}$), and L is the number of looks of the images (or the equivalent number of looks in case of filtered images). Ground-truth information is required to assess the values of $p(nr)$, $p(r)$, TC_{nr} and TC_r , and consequently the threshold t_{opt} to use in the classification. It is shown that the class parameters TC_{nr} or TC_r are linked by a simple relationship to $TC_{max,nr}$ and $TC_{max,r}$, which are the values where the probability density functions (pdf) of TC for the corresponding class is the highest, e.g. for the non-rice class:

$$TC_{nr} = \frac{L+1}{L-1} TC_{max,nr} \quad (2)$$

and likewise for the rice class.

For the case of STC images, equations (1) and (2) do not apply strictly because the pdf of STC is different from the pdf of TC. However, as the pdf of STC cannot be expressed theoretically and is not expected to differ much from that of TC, equations (1) and (2) will be used on the STC.

In the present study, the rice maps retrieved in (Bouvet et al. 2009) from the APP dataset can be used as ground truth over the An Giang province to calculate $p(nr)$, $p(r)$, and to plot the histograms of STC for the rice and the non-rice classes, for Season 2 (Summer-Autumn) and Season 3 (Autumn-Winter), in order to estimate $STC_{max,nr}$ and $STC_{max,r}$. The proportion of rice $p(r)$ calculated in the APP maps is 62.7% for Season 2 and 20.6% for Season 3. The normalized histograms of these seasonal classification features are plotted in Fig. 6 for the two considered classes, based on the pixels identified as rice or non-rice in the maps derived from APP, which have been spatially degraded and projected to the geocoded WSM data. These normalized histograms estimate the pdf of STC for the two classes. The STC_{max} parameters are assessed for each class by identifying the STC value where the histogram is maximal, and the STC_r and STC_{nr} class parameters are retrieved using equation (2). The values corresponding to the optimal classification threshold t_{opt} for Summer-Autumn and Autumn-Winter are then found from (1) to be respectively 4.49dB and 4.53dB.

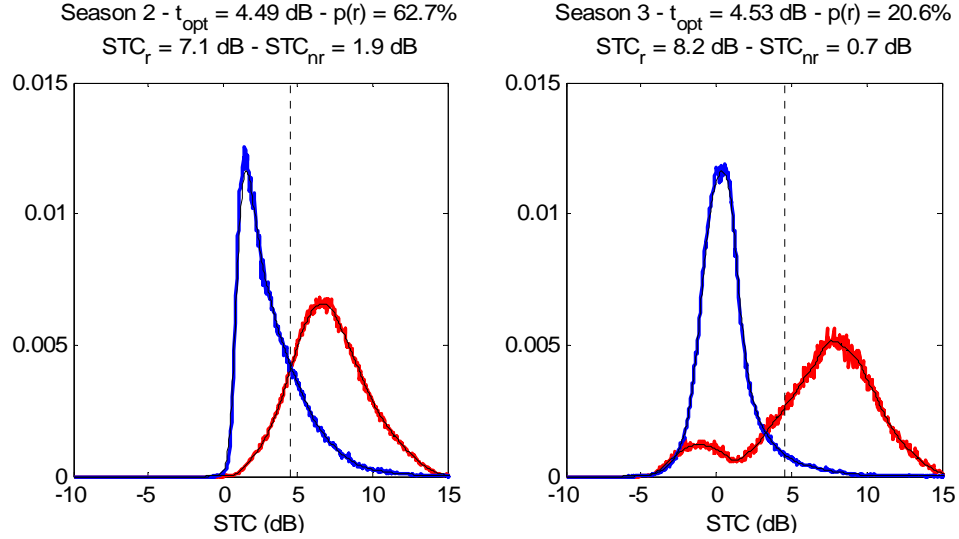


Figure 6. Histograms of the STC classification features for Season 2 (left) and Season 3 (right), for the rice class (red) and the non-rice class (blue). Vertical dashed black lines represent the theoretical optimal classification threshold t_{opt} retrieved from the histograms.

In most applications, no such extensive ground truth data is available. Quite commonly, the location of a few sample areas of rice and non-rice are known and allow an approximate estimation of STC_{nr} and STC_r . The class proportions, $p(nr)$ and $p(r)$, remain however generally unknown and have to be assumed to be equal to 0.5, which leads to a simplified expression of the optimal threshold: $t_{opt} = \sqrt{STC_{nr}STC_r}$. In less favourable cases when no ground information is available at all, like here in the other provinces of the Mekong delta, the theoretical value of the optimal classification threshold cannot be retrieved. In that case, the only option is to use values from literature. Previous studies have suggested a threshold of 3dB (Le Toan et al. 1997; Liew et al. 1998; Ribbes and Le Toan 1999), which can be used as a baseline algorithm. This value is significantly lower than the values around 4.5 dB found for An Giang. Figure 7 presents the pixel-based classification accuracy for the An Giang province, calculated

from the APP-derived maps, as a function of the retained classification threshold, with a particular focus on the true optimal threshold, leading to the maximal accuracy, and on the 3dB threshold. The figure indicates that, for this dataset, a relatively wide range of threshold values - roughly between 3dB and 5dB in Summer-Autumn, and between 3dB and 7dB in Autumn-Winter - lead to similarly high pixel-based accuracies. In particular, the use of the baseline algorithm (3dB threshold) leads to only slightly suboptimal results, with an additional error of about 2% compared to the optimal accuracy. It was therefore chosen to use the 3dB threshold for the mapping of rice areas over the whole Mekong delta.

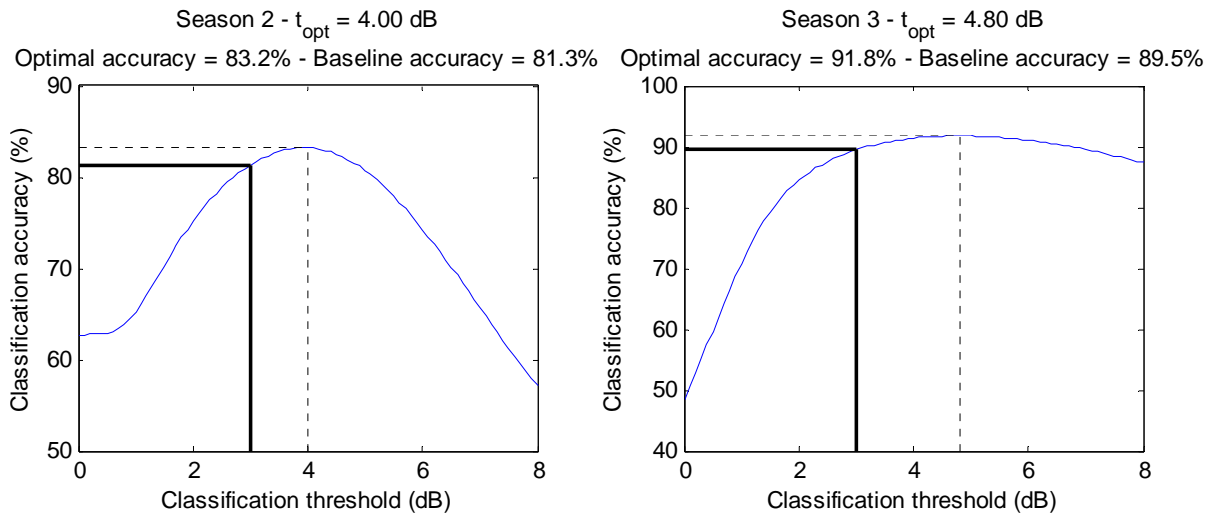


Figure 7. Classification accuracy as a function of the retained classification threshold for season 2 (left) and season 3 (right) in An Giang province. The true optimal threshold t_{opt} , leading to the maximal accuracy, is calculated and plotted in dashed line, and the baseline 3dB threshold and corresponding accuracy are plotted in full bold line.

D. Creating STC images

Because of the lack of WSM images in the end of 2006, the first crop in 2007 - the Winter-Spring crop – cannot be mapped exhaustively. The study therefore focuses on the other rice seasons. One STC image is created for Season 2 (the Summer-Autumn crop) and another one for Season 3 (i.e. both the main wet season and the Autumn-Winter season because of their simultaneity).

In some areas with homogeneous cropping patterns, the simple knowledge of agricultural calendars should be sufficient to select the TC images to be used for the production of the STC images. For the case of the Mekong River Delta however, the variety of cropping patterns and calendars between provinces has to be accounted for. Figure 8 shows intermediate rice maps obtained by considering groups of up to three TC images acquired during a short period of time and belonging to different tracks. The groups are composed of one TC image from track 412 together with the preceding TC image from track 304 (seven days before) and the following TC image from track 32 (nine days later) when available, which corresponds to the lines in Table 4. Pixels in white (values above the 3dB threshold for at least one of the TC images in the group) therefore represent the paddy fields that are at the flooding stage around the indicated date. This reflects well the complexity of the cropping patterns in the region, as at each date, flooded fields are present somewhere in the delta. This enhances the need of a precise selection of the TC images at the province level for the production of STC images.

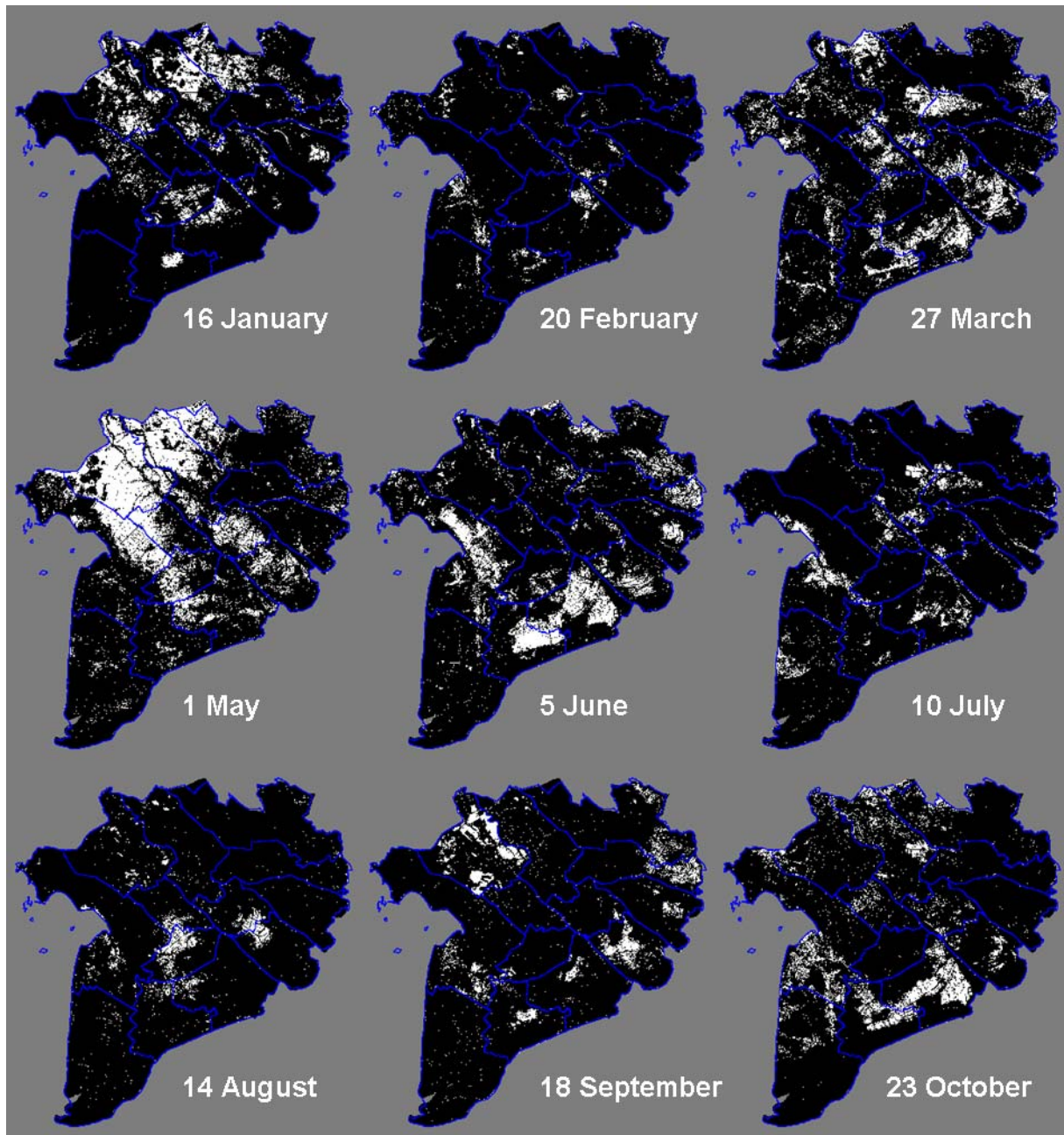


Figure 8. Rice maps derived from nine groups of up to three TC images. Pixels in white represent the pixels with a TC value above the 3 dB threshold for at least one image in the group, and pixels in black with a TC value below the threshold for all the images in the group.

In this study, we chose to use time-series of NDVI as ancillary data to select the TC images. The VGT-S10 products of the VEGETATION-2 instrument on-board SPOT-5 have been used. They consist in 10-day syntheses of the four spectral bands of the instrument at a spatial resolution of 1km. The NDVI, which is the normalized difference of the near infrared and red reflectances, is a proxy for the chlorophyll content within one pixel, and therefore for the live green vegetation. The 36 VGT-S10 products of the year 2007 covering the Mekong Delta were downloaded and processed to produce NDVI time-series. A cloud-removal filter inspired on the Best Index Slope Extraction (BISE) algorithm (Viovy et al. 1992) was applied on the NDVI time-series. The dates of local crop calendars are estimated by a visual interpretation of the vegetation cycles depicted in the NDVI time-series at selected pure pixels among each province. A sufficient number of pixels should be chosen to represent the cropping pattern diversity in each province (i.e. mainly double and triple cropping) and the variety in each cropping pattern (from early to late crops).

IV. RESULTS AND DISCUSSION

A. Mapping results

A 3dB threshold is applied on the two STC images that have been created by keeping the maximum value of the TC images selected within each province for Season 2 and Season 3. The isolated rice pixels or the very small patches detected as rice (less than 40 pixels) are removed from the rice class because they are likely to be errors due to remaining speckle.

Figure 9 shows the rice maps obtained in the whole Mekong delta. The map depicts the areas where rice is grown in Season 2 only in green, in Season 3 only in red, in both seasons in

515 yellow, and the areas where no rice is detected in black. As Season 1 is missing, it is reasonable
516 to assume that in inland provinces, the green areas actually correspond to double-rice patterns
517 and the yellow areas to triple-rice patterns. This map exhibits cropping patterns that are very
518 similar to those presented by (Sakamoto et al. 2006), which include coarser resolution rice maps
519 of 2002 and 2003 derived from MODIS and a land-use map of 2002 provided by the Sub-
520 National Institute for Agricultural Planning and Projection of Vietnam. In particular, in An
521 Giang province, the WSM map illustrates the well-known expansion of triple-rice (labeled as
522 “both seasons” in this case) between 2002-2003 and 2007.
523 Table 5 lists the rice areas for both seasons calculated from these rice maps.

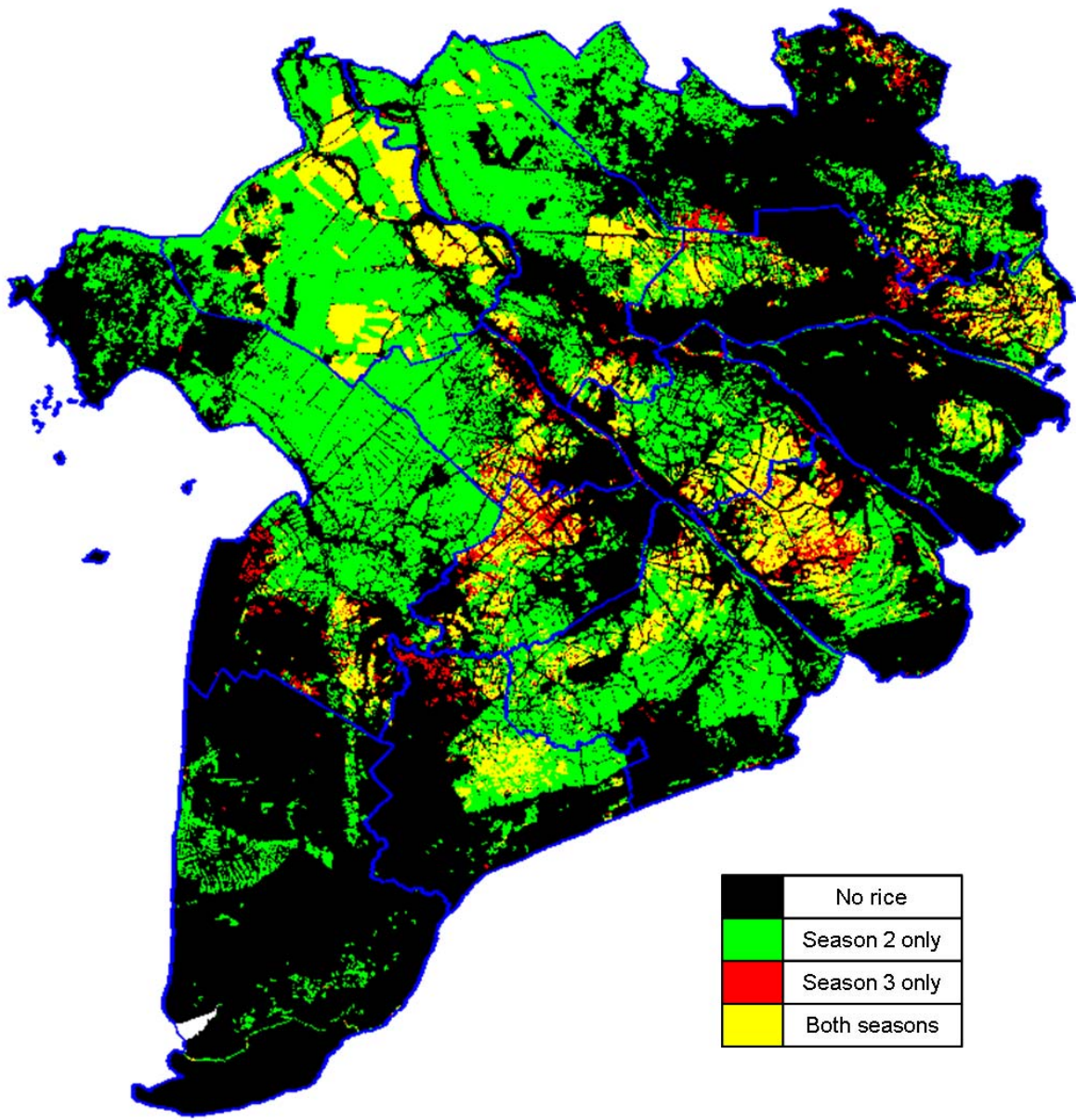


Figure 9. Rice map derived from the STC images for Season 2 and Season 3.

Table 5. Planted area of rice by province (in ha) for Season 2 and Season 3 retrieved from the WSM data

| | Season 2 | Season 3 |
|-------------------|----------|----------|
| Long An | 123461 | 23817 |
| Tiền Giang | 64666 | 39444 |
| Bến Tre | 24531 | 8981 |
| Trà Vinh | 81179 | 54896 |
| Vĩnh Long | 66903 | 25465 |
| Đồng Tháp | 203720 | 32927 |
| An Giang | 263321 | 78725 |
| Kiên Giang | 257890 | 20120 |
| Cần Thơ | 73293 | 21586 |
| Hậu Giang | 56078 | 36819 |
| Sóc Trăng | 155938 | 28954 |
| Bạc Liêu | 67470 | 26635 |
| Cà Mau | 40155 | 795 |

B. Validation

A visual comparison of the rice maps in An Giang is presented in Figure 10 between the new rice maps derived from WSM and the rice maps derived from APP data in a previous study. Although the classification features in the two SAR methods are based on different physical mechanisms, the results compare very well to each other, which demonstrates the robustness of both methods for the identification of rice fields. The pixel-based accuracy, which corresponds to the percentage of pixels that are classified in the same category (rice or non-rice) by the two methods, is equal to 81.3% and 89.5% for Season 2 and Season 3 respectively. When considering the joint mapping results at the two seasons, four classes are distinguished: no rice,

rice in Season 2 only, rice in Season 3 only, and rice in both seasons, similarly to the larger map in Fig. 9. The normalized confusion matrix for the four classes, with the APP map considered as reference data and the WSM map as classification data, is given in Table 6. Each cell in the table contains the percentage of pixels in the scene that are classified in the class defined by its column and by its line in the APP and WSM maps respectively. The overall classification accuracy is therefore equal to the sum of the figures in the diagonal: 75.8%. Most of the classification error is commission error, i.e. pixels classified as non-rice in the APP map are classified as rice in the WSM map (mostly Season 2 and both seasons). Two sources of commission are identified from Fig.10: a) a small part of the rivers are detected as rice by the method based on WSM because the backscattering of water can change with wind conditions, and b) with its coarser spatial resolution, the WSM map is not able to discriminate fine features such as roads and channels between fields. As rivers, roads and channels do not change from year to year, both causes of commission error can be tackled by masking these areas through the use of a GIS land cover database for example.

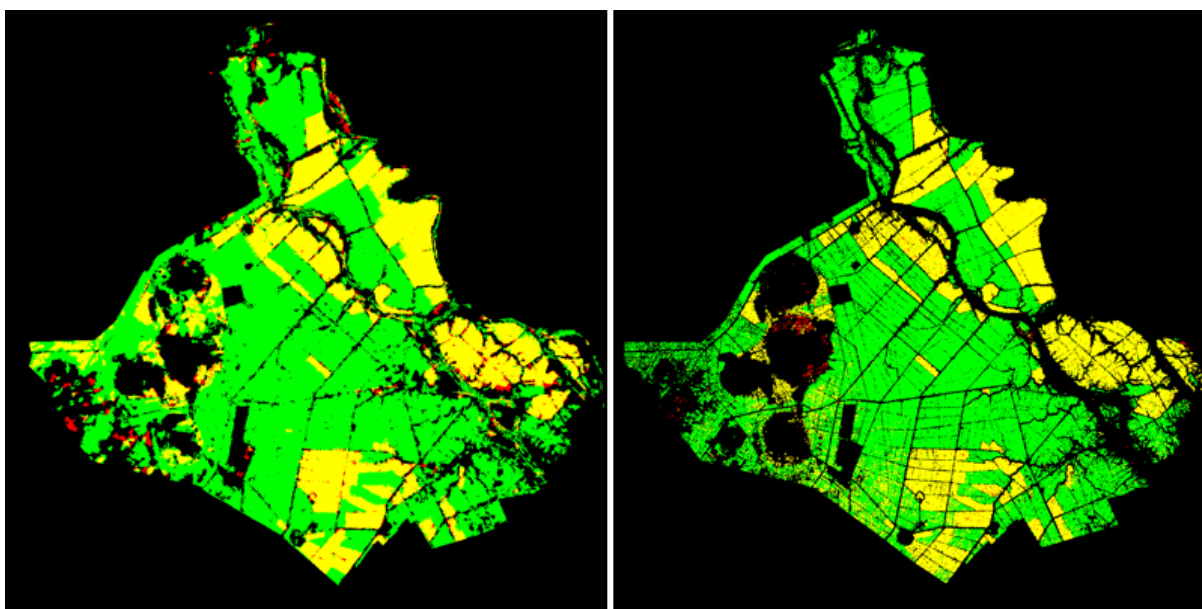


Figure 10. Rice maps derived from the WSM dataset (left) and APP dataset (right) in An Giang for Season 2 and Season 3 in 2007 (same legend as Figure 9).

Table 6. Confusion matrix between classes derived from APP and WSM.

| | | WSM | | | | |
|-----|--------------|---------------|---------------|--------------|---------------|--------|
| | | no rice | season 2 | season 3 | both seasons | |
| APP | no rice | 19,57% | 11,36% | 1,51% | 4,48% | 36,92% |
| | season 2 | 1,69% | 39,45% | 0,12% | 1,23% | 42,49% |
| | season 3 | 0,09% | 0,09% | 0,03% | 0,32% | 0,52% |
| | both seasons | 0,34% | 2,69% | 0,33% | 16,71% | 20,07% |
| | | 21,69% | 53,58% | 1,98% | 22,74% | |

The ability of the new mapping method to retrieve planted areas can be tested against the statistical data given by GSO. As suggested in Table 3, the planted areas given for the Autumn category in the statistics has to be compared to the sum of the planted areas retrieved by WSM for Season 2 and Season 3 in the inland provinces, and to the planted areas retrieved for Season

2 in the coastal provinces. The corresponding figures are plotted in Fig. 11. The two datasets show a very good agreement ($R^2=0.92$) with a root mean square error of 26000 ha per province.

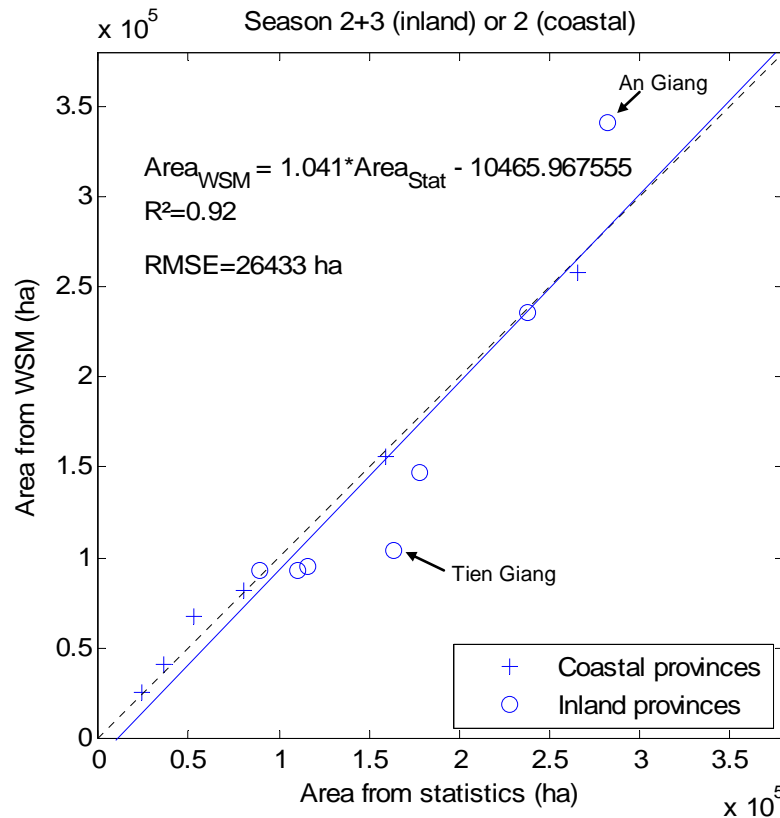


Figure 11. Retrieved rice planted areas per province (in ha) for season 2 (coastal provinces) and the sum of Season 2 and Season 3 (inland provinces) vs. statistical rice planted areas in Autumn.

The blue line represents the linear regression between the two datasets.

C. Discussion

As can be seen from Fig. 11, the area estimation is excellent in coastal provinces and a bit less good in inland provinces. One possible reason for this difference could be that the assumption that the Autumn category from the statistical database contains Season 2 and Season 3 in inland

provinces is not totally valid. There might be differences between inland provinces in the definition of seasons by the General Statistics Office. This must not however hide the fact that true sources of error exist. Some sources of error can lead to an overestimation (up to 59000ha in An Giang) or an underestimation (up to 59000ha in Tiền Giang) of the rice planted areas. These sources include the effect of mixed pixels, commission errors (non-rice areas classified as rice) and omission errors (rice areas classified as non-rice).

Several types of land use can exhibit a high backscatter increase under certain conditions, thus generating commission errors. These cases can generally be easily discarded by a more detailed analysis of the available SAR time-series. For example, in the Mekong River Delta, a rapid increase in backscatter can happen locally when the seasonal flood recedes, or over permanent water areas (lakes, rivers) because of the wind, resulting in an erroneous detection of rice. The seasonal flood should be relatively easily spotted by detecting low backscatter values during several consecutive repeat-pass acquisitions. Permanent water areas on the other hand can be masked out by applying a threshold on the mean backscatter within a SAR time-series. In the rice growing regions where another major crop is grown (e.g. wheat), confusion could also occur when one image is acquired before harvest and the next one after harvest, which could result in a backscatter increase. But in most cases these crops are not grown simultaneously to rice so the confusion can be avoided by selecting the relevant acquisition dates.

The effect of mixed pixels is more important and is directly related to the spatial resolution of the imagery data. In the study area, the agricultural landscape is composed of large surfaces of rice fields separated by smaller non-rice elements such as roads, irrigation channels, dwellings, or vegetable patches, especially in the irrigated areas in the inland provinces. Consequently, many pixels classified as rice actually contain a small proportion of non-rice surface. The

reverse is not true, so mixed pixels globally lead to an overestimation of rice planted areas. This overestimation is more important at coarser resolutions, and has already been illustrated in Fig. 10 for the An Giang province.

The area overestimation due to mixed pixels should also be present in other provinces, but it is not observed in Fig.11. It can be supposed that this overestimation may be at least partially compensated by other error sources that lead to area underestimation, i.e. omission errors. This can happen when SAR data are missing during the few days when the fields are flooded. This is most likely to have happened here for Season 3, when no data could be acquired in track 032.

For the extreme case of Tiền Giang, another factor may be involved. The NDVI time-series of three representative selected pixels in the province are plotted in Fig. 12, after smoothing with a central moving average. They all describe a triple-cropping pattern. The green and blue profiles are typical of the well-known Winter-Spring/Summer-Autumn/Autumn-Winter pattern. In the contrary, the red profile differs from this planting scheme, with a peculiar “Spring-Summer” crop (locally named “Xuân Hè”) inserted between the Winter-Spring and Summer-Autumn seasons, and no Autumn-Winter crop as the area is reached by the seasonal floods in October-November. This Winter-Spring/Spring-Summer/Summer-Autumn pattern is reported in (Tanaka 1995), only in Tiền Giang province. This minor pattern may be badly detected in the STC images designed for Season 2 and Season 3, and the attribution of each of its three crops to the statistical categories (Spring, Autumn, Winter) is unknown. These two effects combined can explain part of the discrepancies between the WSM and statistical figures in Tiền Giang.

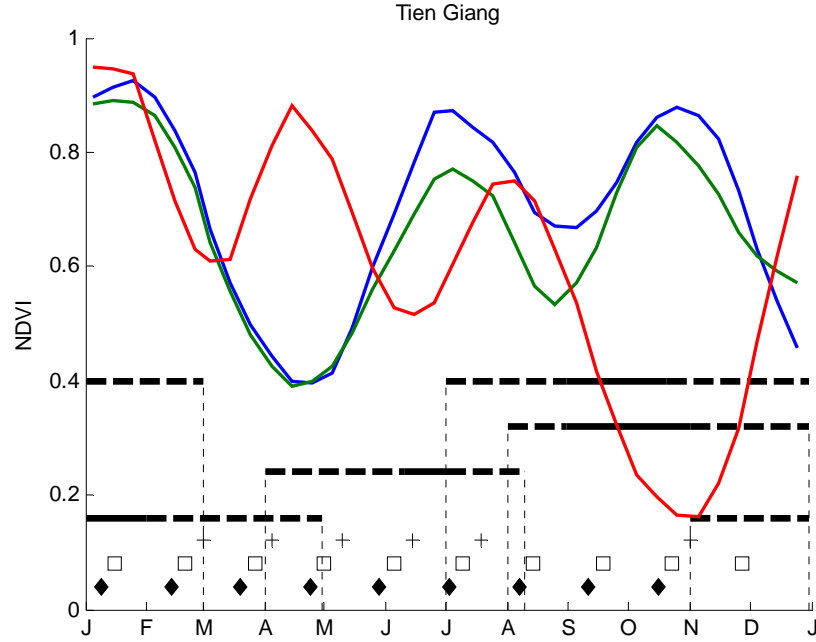


Figure 12. Smoothed NDVI profiles of three pixels representative of the triple-cropping pattern in Tien Giang province. The dates of the WSM images are represented, as well as the typical crop calendar as in Fig. 4.

V. CONCLUSION

A novel rice mapping method has been developed, based on former methods using the temporal backscatter change as a classification feature, and adapted to the use of multi-track wide-swath datasets. The effect of the spatial and temporal variation of the incidence angle within the dataset is tackled by using exclusively temporal change images, which are intensity ratio images of two consecutive acquisitions in the same track. This allows increasing significantly the observation frequency and the size of the mapped areas compared to the former methods using single-track narrow-swath datasets.

639 The study has been conducted in the Mekong River Delta, where rice fields have been mapped
640 over the whole delta for two crops in 2007 (Season 2 and Season 3), using ASAR WSM data.
641 Comparison with a rice map of An Giang province produced with finer-resolution data has
642 shown that the rice detection is very effective with the new methods.

643 Regarding area estimation, an excellent correlation has been obtained when comparing the
644 planted areas retrieved from the rice maps to the planted areas reported in the official statistics.
645 However, this positive result is likely to be due partly to error compensation between
646 overestimation and underestimation sources. As such, the operational use of this method for an
647 accurate area estimation of rice fields should be considered only within an integrated scheme
648 involving other data sources. In well-monitored areas where detailed GIS-based land cover maps
649 are available, which is increasingly common, the method can be applied to the sole pixels known
650 to be agricultural areas in order to reduce commission errors and limit the effect of mixed pixels.

651 In that case, the method can be used as a tool to update this GIS land cover database globally
652 and in near-real time much more effectively than by field investigations. Such operational
653 systems can be based on the data provided by the two existing C-band SARs providing wide-
654 swath data, namely ENVISAT/ASAR and RADARSAT-1 and 2. The limiting factor in this case
655 would be data availability. Given the large choice of operating modes for these sensors,
656 acquisition conflicts between users are very frequent and make it difficult to obtain consistent
657 time-series. For example, in this study, it has been possible to use only three satellite tracks,
658 while under these latitudes, each part of the Earth surface can be observed by 6 tracks in
659 ascending pass and 6 in descending pass, which makes a potential observation interval of about
660 3 days. The effective acquisition of this data would require dedicated strategies from the space
661 agencies. In the future, the Sentinel-1 satellite (planned for launch by the European Space

Agency around 2012) should be able to solve this problem, and is therefore a very promising tool for the operational application of the rice mapping method developed in this article. Although tested here only in the Mekong River Delta, the method should be efficient in every rice-growing region, as long as a flooding stage is present. New farming practices have developed in the last years in Vietnam, consisting in direct sowing of germinated seeds on wet soil rather than transplanting of young plants in flooded fields. In that case still, fields are flooded a few days after sowing, so the mapping method is still valid, but as the flooding period is reduced, the need of frequent imagery acquisitions is even harsher. As the method is based on the detection of an event that occurs at the beginning of the rice growing cycle, it is well-suited to the early assessment of cultivated areas. Therefore, if successfully applied on an operational basis, it would be potentially very useful to national statistics officers, decision makers and rice trade professionals.

ACKNOWLEDGEMENT

The ENVISAT/ASAR data used in this study were provided by the European Space Agency (Cat-1 AO project 697).

REFERENCES

Food and Agriculture Organization of the United Nations, "General status of the system of food and agriculture statistics in Viet Nam", http://www.faorap-apcas.org/vietnam/No2_VNM_1.pdf

685 United Nations Department of Economic and Social Affairs, Population Division, "World
 686 population to 2300",
 687 <http://www.un.org/esa/population/publications/longrange2/WorldPop2300final.pdf>
 688 General Statistics Office of Vietnam, "Structure of used land by province",
 689 http://www.gso.gov.vn/default_en.aspx?tabid=466&idmid=3&ItemID=6135
 690 General Statistics Office of Vietnam, "Agriculture, Fishery and Fishery Statistical Data",
 691 http://www.gso.gov.vn/default_en.aspx?tabid=469&idmid=3
 692 Food and Agriculture Organization of the United Nations, "FAOSTAT",
 693 <http://faostat.fao.org/site/567/default.aspx>
 694 Bouvet, A., Le Toan, T., Floury, N., & Macklin, T. (2010). An end-to-end error model for
 695 classification methods based on temporal change or polarization ratio of SAR intensities.
 696 *IEEE Transactions on Geoscience and Remote Sensing*, 48, 3521-3538
 697 Bouvet, A., Le Toan, T., & Lam Dao, N. (2009). Monitoring of the Rice Cropping System in the
 698 Mekong Delta Using ENVISAT/ASAR Dual Polarisation Data. *IEEE Transactions on*
 699 *Geoscience and Remote Sensing*, 47, 517-526
 700 Chakraborty, M., Manjunath, K.R., Panigrahy, S., Kundu, N., & Parihar, J.S. (2005). Rice crop
 701 parameter retrieval using multi-temporal, multi-incidence angle Radarsat SAR data.
 702 *ISPRS Journal of Photogrammetry & Remote Sensing*, 59, 310-322
 703 Chen, C., & McNairn, H. (2006). A neural network integrated approach for rice crop
 704 monitoring. *International Journal of Remote Sensing*, 27, 1367-1393
 705 Chen, J., Lin, H., & Pei, Z. (2007). Application of ENVISAT ASAR data in mapping rice crop
 706 growth in Southern China. *IEEE Geoscience and Remote Sensing Letters*, 4, 431-435

707 Frohking, S., Qiu, J., Boles, S., Xiao, X., Liu, J., Zhuang, Y., Li, C., & Qin, X. (2002).
708 Combining remote sensing and ground census data to develop new maps of the
709 distribution of rice agriculture in China. *Global Biogeochemical Cycles*, 16

710 Inoue, Y., Kurosu, T., Maeno, H., Uratsuka, S., Kozu, T., Dabrowska-Zielinska, K., & Qi, J.
711 (2002). Season-long daily measurements of multifrequency (Ka, Ku, X, C, and L) and
712 full-polarization backscatter signatures over paddy rice field and their relationship with
713 biological variables. *Remote Sensing of Environment*, 81, 194-204

714 Kurosu, T., Fujita, M., & Chiba, K. (1995). Monitoring of rice crop growth from space using the
715 ERS-1 C-band SAR. *IEEE Transactions on Geoscience and Remote Sensing*, 33, 1092-
716 1096

717 Le Toan, T., Laur, H., Mougin, E., & Lopes, A. (1989). Multitemporal and dual-polarization
718 observations of agricultural vegetation covers by X-band SAR images. *IEEE*
719 *Transactions on Geoscience and Remote Sensing*, 27, 709-718

720 Le Toan, T., Ribbes, F., Wang, L.-F., Floury, N., Ding, K.-H., Kong, J.A., Fujita, M., & Kurosu,
721 T. (1997). Rice crop mapping and monitoring using ERS-1 data based on experiment and
722 modelling results. *IEEE Transactions on Geoscience and Remote Sensing*, 35, 41-56

723 Liew, S.C., Kam, S.-P., Tuong, T.-P., Chen, P., Minh, V.Q., & Lim, H. (1998). Application of
724 multitemporal ERS-2 synthetic aperture radar in delineating rice cropping systems in the
725 Mekong River Delta, Vietnam. *IEEE Transactions on Geoscience and Remote Sensing*,
726 36, 1412-1420

727 Lopes, A., Touzi, R., & Nezry, E. (1990). Adaptive speckle filters and scene heterogeneity.
728 *IEEE Geoscience and Remote Sensing Letters*, 28, 992-1000

729 Lopez-Sanchez, J.M., Ballester-Berman, J.D., & Hajnsek, I. (2010). First results of rice
 730 monitoring practices in Spain by means of time series of TerraSAR-X dual-pol images.
 731 *IEEE Journal of Selected Topics in Applied Earth Observations and Remote Sensing*, in
 732 *press*
 733 Ribbes, F., & Le Toan, T. (1999). Rice field mapping and monitoring with RADARSAT data.
 734 *International Journal of Remote Sensing*, 20, 745-765
 735 Rignot, E., & van Zyl, J. (1993). Change detection techniques for ERS-1 SAR data. *IEEE*
 736 *Transactions on Geoscience and Remote Sensing*, 31, 896-906
 737 Rosenqvist, A. (1999). Temporal and spatial characteristics of irrigated rice in JERS-1 L-band
 738 SAR data. *International Journal of Remote Sensing*, 20, 1567-1587
 739 Sakamoto, T., Nguyen, N.V., Ohno, H., Ishitsuka, N., & Yokozawa, M. (2006). Spatio-temporal
 740 distribution of rice phenology and cropping systems in the Mekong Delta with special
 741 reference to the seasonal water flow of the Mekong and Bassac rivers. *Remote Sensing of*
 742 *Environment*, 100, 1-16
 743 Shao, Y., Fan, X., Liu, H., Xiao, J., Ross, S., Brisco, B., Brown, R., & Staples, G. (2001). Rice
 744 monitoring and production estimation using multitemporal RADARSAT. *Remote*
 745 *Sensing of Environment*, 76, 310-325
 746 Tanaka, K. (1995). Transformation of rice-based cropping patterns in the Mekong Delta: From
 747 intensification to diversification. *Southeast Asian Studies*, 33, 363-378
 748 Viovy, N., Arino, O., & Belward, A. (1992). The Best Index Slope Extraction (BISE): A
 749 method for reducing noise in NDVI time-series. *International Journal of Remote*
 750 *Sensing*, 13, 1585-1590

751 Wang, L.-F., Kong, J.A., Ding, K.-H., Le Toan, T., Ribbes-Baillarin, F., & Floury, N. (2005).
752 Electromagnetic scattering model for rice canopy based on Monte Carlo simulation.
753 *Progress In Electromagnetics Research*, 153-171

754 Xiao, X., Boles, S., Frolking, S., Li, C., Babu, J.Y., Salas, W., & Moore III, B. (2006). Mapping
755 paddy rice agriculture in South and Southeast Asia using multi-temporal MODIS images.
756 *Remote Sensing of Environment*, 100, 95-113

757 Xiao, X., Boles, S., Frolking, S., Salas, W., Moore III, B., & Li, C. (2002a). Observation of
758 flooding and rice transplanting of paddy rice fields at the site to landscape scales in
759 China using VEGETATION sensor data. *International Journal of Remote Sensing*, 23,
760 3009-3022

761 Xiao, X., Boles, S., Frolking, S., Salas, W., Moore III, B., Li, C., He, L., & Zhao, R. (2002b).
762 Landscape-scale characterization of cropland in China using Vegetation and Landsat TM
763 images. *International Journal of Remote Sensing*, 23, 3579-3594

764 Xiao, X., Boles, S., Liu, J., Zhuang, D., Frolking, S., Li, C., Salas, W., & Moore III, B. (2005).
765 Mapping paddy rice agriculture in southern China using multi-temporal MODIS images.
766 *Remote Sensing of Environment*, 95, 480-492

767

768